

**TiO<sub>2</sub>-SnO<sub>2</sub>:F interfacial electronic structure investigated by soft x-ray absorption spectroscopy**Coleman X. Kronawitter,<sup>1,2</sup> Mukes Kapilashrami,<sup>3</sup> Jonathan R. Bakke,<sup>4</sup> Stacey F. Bent,<sup>4</sup> Cheng-Hao Chuang,<sup>3,5</sup> Way-Faung Pong,<sup>5</sup> Jinghua Guo,<sup>3</sup> Lionel Vayssieres,<sup>6,\*</sup> and Samuel S. Mao<sup>1,2,†</sup><sup>1</sup>*Department of Mechanical Engineering, University of California at Berkeley, Berkeley, California 94720, USA*<sup>2</sup>*Environmental Energy Technologies Division, Lawrence Berkeley National Laboratory, Berkeley, California 94720, USA*<sup>3</sup>*Advanced Light Source, Lawrence Berkeley National Laboratory, Berkeley, California 94720, USA*<sup>4</sup>*Department of Chemical Engineering, Stanford University, Stanford, California 94305, USA*<sup>5</sup>*Department of Physics, Tamkang University, Tamsui, Taiwan, Republic of China*<sup>6</sup>*International Research Center for Renewable Energy, State Key Laboratory of Multiphase Flow in Power Engineering, Xi'an Jiaotong University, Shaanxi 710049, People's Republic of China*

(Received 5 November 2011; revised manuscript received 31 January 2012; published 9 March 2012)

The electronic structure of the titanium dioxide (TiO<sub>2</sub>)-fluorine-doped tin dioxide (SnO<sub>2</sub>:F) interface is investigated by soft x-ray absorption spectroscopy using synchrotron radiation. The measurements probe the site- and symmetry-selected unoccupied density of states and reflect the interaction between an early transition-metal-oxide (*d*<sup>0</sup>) semiconductor and a post-transition-metal-oxide (*d*<sup>10</sup>) degenerate semiconductor. The distinct interfacial electronic structure of TiO<sub>2</sub>-SnO<sub>2</sub>:F is established by contrasting spectra with those for anatase and rutile TiO<sub>2</sub>, SnO<sub>2</sub>:F, and ZnO-SnO<sub>2</sub>:F and CdO-SnO<sub>2</sub>:F interfaces. Oxygen 1s absorption spectra, which relate to the O 2*p* partial density of states of the conduction band, indicate that the interface is associated with a reduction in Ti *d*-O *p* orbital hybridization and an alteration of the TiO<sub>2</sub> crystal field. These observations are consistent with measured titanium 2*p* absorption spectra, which in addition provide evidence for distortion of long-range order around the cation site in the interfacial TiO<sub>2</sub>. The TiO<sub>2</sub>-SnO<sub>2</sub>:F interface is a functional component of a number of optoelectronic devices, perhaps most notably within the anode structure of solar cell architectures. In nonequilibrium conditions, such as those found in operating solar cells, interfacial electronic structure directly influences performance by modifying, for instance, the quasi-Fermi level electrons and the potential distribution at the transparent electrode.

DOI: [10.1103/PhysRevB.85.125109](https://doi.org/10.1103/PhysRevB.85.125109)

PACS number(s): 73.20.-r, 78.70.Dm

**I. INTRODUCTION**

Performance in modern optoelectronics is increasingly reliant on the efficiency of interfacial processes, which are directly influenced by the character and occupancy of electronic states near the interface. Devices designed to absorb or emit light contain layers of organic or inorganic heterostructures, which either function as active components or which facilitate the extraction or injection of electrons from or to the optically active phases. The interfacial regions of heterostructures, which can extend several nanometers beyond their actual atomic interfaces, can be characterized by abrupt or gradual changes in chemical, structural, and electronic properties.<sup>1</sup> The nature of these atomic- and molecular-level interactions is not restricted to academic interest; the macroscopic performance of modern technologies is often reliant on their presence. Here we can consider, for example, the various incarnations of the excitonic solar cell<sup>2</sup> and its inorganic counterpart the quantum dot solar cell,<sup>3</sup> whose very operation requires exciton dissociation and electron transfer processes, which are interfacial phenomena. In general the significance of heterostructure properties is amplified in nanodevices, the large junction areas within which contribute considerably to the overall device functionality.

In transition-metal-oxide heterostructures, charge transfer, covalent bonding, and orbital reconstruction effects modify the *d* orbital character and occupancy at the interface.<sup>4</sup> These effects are expressed through a number of new discoveries whose related technologies will rely on precise knowledge of the interface electronic structure, such as those using interfacial

conductivity,<sup>5</sup> magnetism,<sup>6</sup> or electron enrichment.<sup>7</sup> Size effects in low-dimensional oxides further influence interfacial chemistry<sup>8</sup> and electronic structure through enhancements in orbital hybridization<sup>9</sup> and through quantum confinement.<sup>10</sup>

Here we study the electronic structure of the interface of titanium dioxide (TiO<sub>2</sub>) and fluorine-doped tin dioxide (SnO<sub>2</sub>:F, FTO), one of the most commonly used transparent conductive oxides (TCO). SnO<sub>2</sub>:F is the preferred TCO for numerous optoelectronic applications and is notable for its thermal stability over a wide range of processing temperatures. The buried interfaces are studied by synchrotron-based soft x-ray absorption spectroscopy (XAS), which provides spectra related to the site- and symmetry-selected unoccupied density of states. The key experimental requirement is the deposition of ultrathin layers, whose feature dimensions should not exceed the inelastic mean-free path of electrons (~1–10 nm). This enables the measurement of electron yields generated from transitions originating exclusively from the interfacial region upon synchrotron soft x-ray irradiation. For comparative purposes we examine some aspects of CdO- and ZnO-SnO<sub>2</sub>:F interfaces (all post-transition-metal oxides), mainly to highlight the relative chemical sensitivity and specificity of the TiO<sub>2</sub> phase. ZnO and CdO to refer to the binary post-transition-metal oxides, which are expected to remain stoichiometric in these conditions due to the very high ionization potentials of monovalent cations. The TiO<sub>2</sub> phase is strongly influenced by the substrate as will be discussed in detail herein. However, for convenience we refer to the ultrathin titanium oxide as TiO<sub>2</sub>, given that similar preparation conditions for thicker films produce stoichiometric TiO<sub>2</sub>.<sup>11</sup>

Comprehensive understanding of the electronic structure of oxide-TCO interfaces contributes to continuing efforts to optimize a number of optoelectronic devices of considerable social consequence. The oxide-TCO interface can be found in dye-sensitized,<sup>12–14</sup> quantum dot-sensitized,<sup>15</sup> organic,<sup>16</sup> and solid-state solar cells,<sup>17–19</sup> in light-emitting<sup>20</sup> and organic light-emitting diodes, as well as in solar water-splitting photoanodes.<sup>21</sup> In nanodevices the interface may result from the direct growth of nanostructures onto TCO electrodes<sup>22</sup> or through the use of seed layers<sup>23</sup> to facilitate nanostructure growth. In all cases, during device operation electrons are transported through the interfacial region, where they interact with the interface electronic structure. For instance, in dye-sensitized solar cells the open-circuit potential can be limited by recombination at the metal-oxide-TCO interface.<sup>24</sup> Additionally it has recently been demonstrated that annealing  $\alpha$ -Fe<sub>2</sub>O<sub>3</sub> photoanodes at high temperatures for a few minutes alters the nature of the  $\alpha$ -Fe<sub>2</sub>O<sub>3</sub>-TCO interface, leading to a dramatic increase in water oxidation photocurrents in photoelectrochemical cells.<sup>25</sup> Another recent report, which has motivations similar to those in this study, has characterized the TiO<sub>2</sub>-indium tin oxide (ITO) interface electronic structure by low intensity x-ray and UV photoemission spectroscopy.<sup>26</sup> A fundamental understanding of the oxide-TCO interface provides direction to address operational deficiencies at their physical source. To best facilitate these important fields, we fabricated heterostructures using techniques that realistically represent actual fabrication steps for these devices: use of commercial polycrystalline SnO<sub>2</sub>:F substrates, low temperatures, and moderate pressures.

## II. EXPERIMENT

Ultrathin films of TiO<sub>2</sub>, ZnO, and CdO were fabricated by atomic layer deposition (ALD). Films were deposited onto commercial SnO<sub>2</sub>:F substrates (Pilkington, TEC 7) at 150 °C using commercial titanium tetrachloride, diethyl zinc, dimethyl cadmium, and water as the precursors. The pulsing sequence for each system was 3-s metal molecule, 60-s N<sub>2</sub> purge, 3-s water, and 60-s N<sub>2</sub> purge, where the N<sub>2</sub> purge and carrier flow rate is constant at 80 standard cubic centimeters per minute (SCCM). Six cycles of ZnO and CdO and 15 cycles of TiO<sub>2</sub> were performed so that the thickness of each oxide is  $12 \pm 2$  Å.<sup>11,27</sup> Prior to measurement, all samples were annealed in air at 450 °C for 2 h (0.36 °C s<sup>-1</sup> ramp rate from 23 °C to 450 °C) to ensure the crystallinity of all phases.

Soft x-ray absorption spectra were measured on Beamline 8.0 at the Advanced Light Source (ALS) at Lawrence Berkeley National Laboratory. Spectra were recorded in total electron yield mode (TEY) and were obtained by measurement of the sample drain photocurrent under irradiation with monochromatic light. The resolutions of the measurements were 0.4 eV at the O *K*-edge, 0.35 eV at the Sn *M*-edge, and 0.3 eV at the Ti *L*-edge. The incident radiation flux was monitored by the photocurrent produced in a gold mesh in the beam path. The photon energy was calibrated using the first peak of the anatase TiO<sub>2</sub> O *1s* absorption spectrum located at 530.8 eV. The presented absorption spectra for anatase and rutile TiO<sub>2</sub> were measured on Beamline 7.0.1.

## III. RESULTS AND DISCUSSION

XAS probes the site- and symmetry-selected unoccupied density of states through an electronic transition between a localized core state and a valence state in a transition metal oxide system. The large energy separation among core levels gives the technique elemental selectivity, the participation of valence electrons yields chemical state sensitivity, and the dipole nature of the transitions provides symmetry information. The probe is localized to one specific atomic site, around which the electronic structure is reflected as a partial density of states contribution.

To provide context to an analysis of interfacial x-ray absorption spectra, a few important distinctions are necessary to be made between TiO<sub>2</sub> and the post-transition-metal-oxides SnO<sub>2</sub>, ZnO, and CdO. In bulk TiO<sub>2</sub>, Ti ions have a Ti<sup>4+</sup>(3*d*<sup>0</sup>) electronic configuration, and the empty conduction band is comprised of Ti 3*d*, 4*s*, and 4*p* orbitals, with 3*d* orbitals dominant in the bottom of the conduction band. In contrast, in SnO<sub>2</sub> for example, Sn ions have a Sn<sup>4+</sup>(4*d*<sup>10</sup>5*s*<sup>0</sup>5*p*<sup>0</sup>) configuration, with 5*s* and 5*p* orbitals dominant in the conduction band minimum.<sup>28</sup> In addition, with a few exceptions the post-transition-metal-oxide cations have one preferred oxidation state; whereas in the transition-metal oxides, there is often a small energy difference between the *d*<sup>*n*</sup> and *d*<sup>*n*+1</sup> configurations. As a result, the transition metals typically have many stable oxides, and their surface and interface chemistry is much more complex.<sup>29</sup> These complexities are evident in x-ray absorption spectra; their interpretation requires the inclusion of titanium oxide reference spectra. There are additional properties specific to the reference oxides examined, which must be briefly addressed. The anisotropy<sup>30</sup> and surface polarity<sup>31</sup> of ZnO are important aspects of this material, which directly influence electronic structure measurements. Additionally, the large electron accumulation in CdO,<sup>32</sup> associated with massive band bending, is not characteristic of TiO<sub>2</sub> and should be noted. These factors should not influence our interpretations to any significant degree.

### A. Oxygen 1s soft x-ray absorption

Upon irradiation of the oxides with x-rays of sufficient energies, core O *1s* electrons are promoted to an excited state, which is coupled to the original state by the dipole selection rule.<sup>33</sup> The change in angular momentum quantum number ( $\Delta L$ ) must be  $\pm 1$ —only the oxygen *p* character is probed. The existence of these transitions in itself is an indication of the partially covalent bonding in these materials.<sup>34</sup> For this application, O *1s* spectra provide a useful representation of the unoccupied electronic structure at interfacial metal sites, because in these materials, above the Fermi level empty bands are predominantly metal weight hybridized with O 2*p* character.

The O *1s* absorption spectra for the bare SnO<sub>2</sub>:F surface and the TiO<sub>2</sub>-SnO<sub>2</sub>:F, ZnO-SnO<sub>2</sub>:F, and CdO-SnO<sub>2</sub>:F interfaces are provided in Fig. 1. The qualitatively similar spectrum measured for all cases confirms the validity of the ultrathin film approach to probe the interface: the buried SnO<sub>2</sub>:F dominates the expression of O *p* states in each XAS measurement. In other words, because the inelastic mean-free path is restricted to  $\sim 1$ –10 nm, the signal represents the O *p* states of the interface, defined as a region approximately 2 nm on either side of the atomic interface.

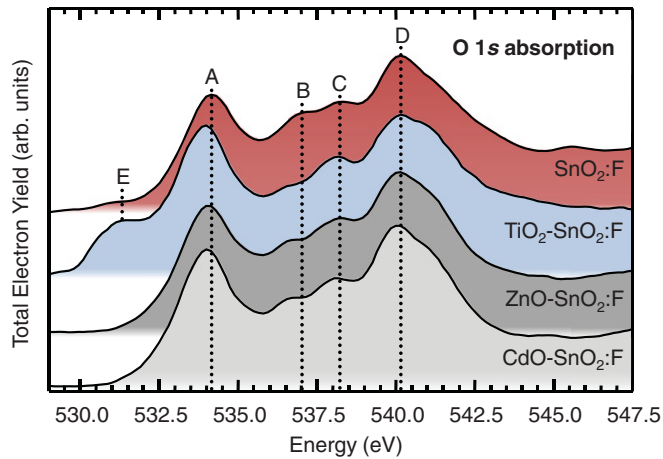


FIG. 1. (Color online) O  $K$ -edge x-ray absorption spectra for (from top to bottom) SnO<sub>2</sub>:F and the TiO<sub>2</sub>-SnO<sub>2</sub>:F, ZnO-SnO<sub>2</sub>:F, and CdO-SnO<sub>2</sub>:F interfaces.

The bottom of the conduction band of SnO<sub>2</sub> is comprised of Sn 5s orbitals, which hybridize with O 2p orbitals and are expressed in the O 1s absorption spectra as peak A in Fig. 1. Peaks B, C, and D primarily correspond to the O 2p orbitals hybridized with Sn 5p orbitals deeper in the conduction band.<sup>35</sup> In the molecular orbital framework, peak A corresponds to transition to the  $a_g$  state, and peaks B, C, and D correspond to the successive transitions to the  $b_{1u}$ ,  $b_{2u}$ , and  $b_{3u}$  states.<sup>36</sup> The  $a_g$  state reflects the partial density of states of the O<sub>2</sub> set of oxygen orbitals, which are perpendicular to the plane of the Sn<sub>3</sub>O trigonal configuration, while the  $b_{1u}$ ,  $b_{2u}$ , and  $b_{3u}$  states reflect a combination of the in-plane O<sub>1</sub> set and out-of-plane O<sub>2</sub> set.<sup>35,37</sup> Peak E, located in the pre-edge region at 531.4 eV, is found uniquely in TiO<sub>2</sub>-SnO<sub>2</sub>:F, and results from the hybridization of unoccupied Ti  $d(t_{2g})$  levels with O 2p levels, which exist in the conduction bands of titanium oxides, as will be discussed in detail later in this paper. Close inspection of the rising edge of peak A reveals additional intensity near 533.4 eV for all thin-film samples. This is attributed to Ti 3d-, Zn 4s-, and Cd 5s-O 2p hybridized states, which exist in the respective conduction bands of the oxides.

### B. Tin 3d soft x-ray absorption

The Sn  $M_{4,5}$ -edge x-ray absorption spectra, presented in Fig. 2, describe transitions from Sn 3d levels to p or f states in the conduction band of SnO<sub>2</sub>:F. The lower signal-to-noise ratio in comparison to those for O  $K$ -edge spectra results from the much lower x-ray absorption cross section of the  $M$ -edge. The conduction band minimum of SnO<sub>2</sub> is dominantly comprised of Sn 5s levels. Deeper in the conduction band the density of states is dominantly Sn p character.<sup>38</sup>

It is apparent in Fig. 2 that Sn 3d absorption at the surface of SnO<sub>2</sub>:F is largely unchanged by the formation of an interface with CdO and ZnO. Here we can consider the relative chemical stability of the post-transition-metal oxides. High energies are required to add or remove electrons when these cations are coordinated with O<sup>2-</sup> ligands, limiting the number of states accessible for the formation of defects, which have different electron configurations.<sup>29</sup> These spectra contrast with that of

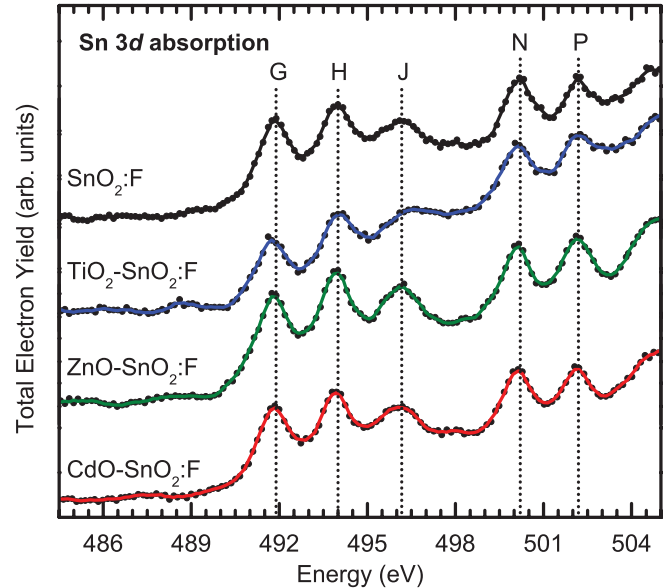


FIG. 2. (Color online) Sn  $M_{4,5}$ -edge absorption spectra for bare SnO<sub>2</sub>:F (black solid line) and the TiO<sub>2</sub>-SnO<sub>2</sub>:F (blue solid line), ZnO-SnO<sub>2</sub>:F (green solid line), and CdO-SnO<sub>2</sub>:F (red solid line) interfaces.

TiO<sub>2</sub>-SnO<sub>2</sub>:F, which contains a large distortion of the  $M_4$  and  $M_5$  bands. The broadening and overall reduction in resolution of these peaks compared to those for bare SnO<sub>2</sub>:F has been found in x-ray absorption spectra for SnO.<sup>39</sup> Through consideration of high-surface-area SnO<sub>2</sub> aerogels, Kucheyev *et al.*<sup>39</sup> assigned the distortion to the presence of undercoordinated surface atoms. Ahn *et al.*<sup>40</sup> observed a similar broadening in their study of size-controlled SnO<sub>2</sub> nanoparticles, where increased broadening was found to be correlated with decreasing nanoparticle size. Broadening in this case was attributed to decreasing long-range order in SnO<sub>2</sub> crystals.

The small leading edge feature at 488.5 eV present in the  $M_5$  band for TiO<sub>2</sub>-SnO<sub>2</sub>:F has been identified previously in SnO<sub>2</sub> aerogels<sup>39</sup> and nanoribbons.<sup>41</sup> It is suggested to be related to Sn p states that are created by oxygen vacancies and surface reconstruction. The spin-orbit splitting creates an  $M_4$  band counterpart that overlaps with peak J, which explains the dramatic distortion of this peak in our experiments. Surface reconstruction of this type will alter the Fermi level position of the heterostructure.<sup>39</sup> The presence of additional Sn p states, which have been assigned to exist both below<sup>42</sup> and above<sup>39</sup> the conduction band minimum, potentially alters the electronic structure of the conduction band. In order to confirm the presence of SnO<sub>2</sub> surface reconstruction, which is only observed indirectly here, more detailed analyses are required, for example, those involving high-resolution transmission electron microscopy.

### C. Titanium 3d band projected onto O 2p orbitals

The strong intensity of peak E in Fig. 1, which corresponds primarily to unoccupied O 2p states, weight-hybridized in states with Ti 3d character,<sup>9</sup> enables a more detailed analysis of the conduction band minimum of TiO<sub>2</sub> at its interface with SnO<sub>2</sub>:F. The difference spectrum obtained by subtraction of the



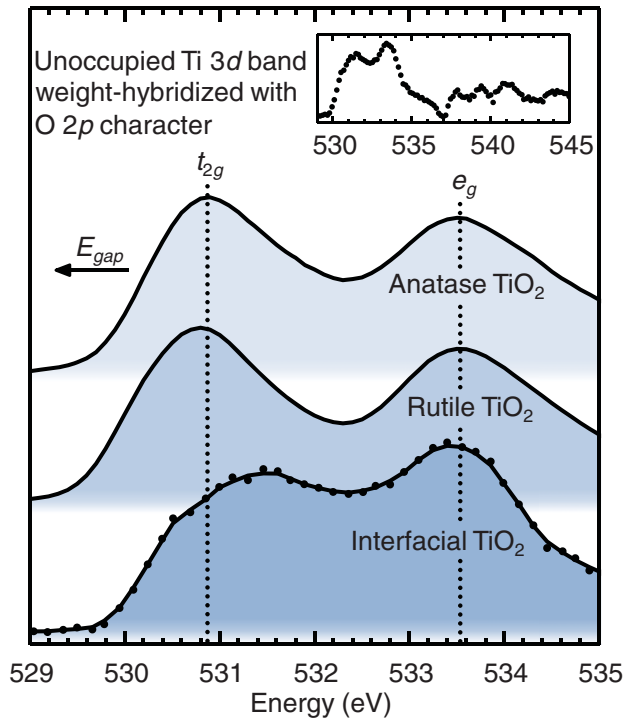


FIG. 3. (Color online) Oxygen 1s absorption spectra for anatase TiO<sub>2</sub>, rutile TiO<sub>2</sub>, and TiO<sub>2</sub> thin film deposited on SnO<sub>2</sub>:F. The interfacial TiO<sub>2</sub> spectrum was obtained by subtraction of the SnO<sub>2</sub>:F O 1s absorption spectrum such that the intensity remained positive. The dashed vertical lines indicate the energies of the Ti  $t_{2g}$  and  $e_g$  band maxima for anatase TiO<sub>2</sub>. The inset provides the interfacial TiO<sub>2</sub> spectrum at higher energies.

SnO<sub>2</sub>:F O 1s absorption spectrum from that of TiO<sub>2</sub>-SnO<sub>2</sub>:F (such that the resulting spectrum intensity is positive) is presented in Fig. 3, with O 1s absorption spectra of anatase and rutile TiO<sub>2</sub> included for comparison. The Ti 3d band of the O 1s absorption spectrum (located from 529 to 535 eV<sup>7</sup>) is of primary interest to this study, and the difference spectrum in this energy range possesses a high signal-to-noise ratio, highlighting the importance of synchrotron-based soft XAS for studying  $d^0$  materials. The 4sp band is located at higher energies (inset of Fig. 3) and possesses a larger energy spread, which is related to the degree of covalency in the material.<sup>33</sup> Increased broadening of this band is consistent with previous investigations of size effects in TiO<sub>2</sub>,<sup>9</sup> as described in detail below. It is possible that the O 1s absorption spectrum of the underlying SnO<sub>2</sub>:F, modified by the presence of the TiO<sub>2</sub>, is not the same as that of bare SnO<sub>2</sub>:F (see discussion above on the Sn  $M$ -edge). The analysis of the difference spectrum that follows is conducted in the context of this unavoidable limitation.

In the oxides of titanium, Ti cations are surrounded by a distorted octahedron of oxygen anions, and the associated electrostatic fields split the  $d$  orbitals into a triply degenerate  $t_{2g}$  band ( $d_{xy}$ ,  $d_{xz}$ , and  $d_{yz}$  orbitals) and a doubly degenerate  $e_g$  band ( $d_{x^2-y^2}$  and  $d_{z^2}$  orbitals). The dashed vertical lines in Fig. 3 show the positions of the  $t_{2g}$  and  $e_g$  bands hybridized with O 2p orbitals in the conduction band of anatase TiO<sub>2</sub>. The energies of the peak maxima corresponding to the  $e_g$  bands nearly overlap among anatase TiO<sub>2</sub>, rutile TiO<sub>2</sub>, and

TiO<sub>2</sub>-SnO<sub>2</sub>:F. In contrast, the centroid of the  $t_{2g}$  peak for TiO<sub>2</sub>-SnO<sub>2</sub>:F lies at greater energies than those for the reference titanium oxides.

The energy separation between the O 2p weights of the  $t_{2g}$  and  $e_g$  sub-bands is a reflection of the ligand-field strength or the ligand-field splitting parameter  $\Delta$ .<sup>33</sup> This parameter depends on the specific metal and ligand involved, as well as the oxidation state of the metal, and in general for a given metal the ligand-field strength increases with increasing oxidation state. In the TiO<sub>2</sub>-SnO<sub>2</sub>:F interface, structural distortions in the lattice could change the symmetry of the cation site environment, which would be associated with a change in the ligand field. Interestingly, Soriano *et al.*<sup>43</sup> showed that structural disorder in TiO<sub>2</sub> induced by surface sputtering is associated with a 0.6-eV reduction in the ligand-field splitting, which was attributed to weaker Ti 3d-O 2p hybridization.

An alteration of the titanium oxide ligand field is notable in this analysis of the interface electronic structure: the field influences the orientation of  $d$  orbitals around the metal ion in transition-metal-oxide systems and by extension many of the system's physical properties. A large deviation of the ligand field at the TiO<sub>2</sub>-SnO<sub>2</sub>:F interface from that of reference TiO<sub>2</sub> will influence electron conduction, which primarily takes place in empty Ti 3d orbitals. Significant alterations of the ligand-field strength suggest the presence of further distortion of the octahedral coordination of Ti.

The line shape of O 1s absorption spectra in this energy range is additionally modified by size effects related to the high density of interface and surface states in nanoscale systems. Recently the size effect on the orbital character of anatase TiO<sub>2</sub> nanoparticles over two orders of magnitude in average diameter (2–200 nm) has been reported.<sup>9</sup> It was determined that as a consequence of the contracted nature of  $d$  orbitals, the hybridization of O 2p with Ti 4s orbitals contributes more significantly in systems with nanoscale dimensionality and high concentrations of surface states. It is reasonable to assume in the present case that interface and surface states manifest as line broadening in the measured O 1s absorption spectra, consistent with a relative enhancement of  $s$ - $p$  orbital hybridization.

#### D. Titanium 2p soft x-ray absorption

Titanium  $L$ -edge absorption spectra were recorded to provide additional information on the interfacial cation site environment of TiO<sub>2</sub>-SnO<sub>2</sub>:F. For comparison, as above, spectra were recorded for anatase and rutile TiO<sub>2</sub> reference crystals. These spectra, presented in Fig. 4(a), possess four primary peaks, which result from the core-hole spin-orbit splitting of 2p levels and the crystal-field splitting of  $d$  orbitals discussed above.<sup>44–47</sup> Specifically, the  $L_3$  band, located from 456 to 462 eV, represents the  $2p_{3/2} \rightarrow 3d_{4s}$  transition; the  $L_2$  band located from 462 to 468 eV represents the  $2p_{1/2} \rightarrow 3d_{4s}$  transition. Peaks  $T$  and  $W$  reflect transitions to empty  $t_{2g}$  levels, and peaks  $U$ ,  $V$ , and  $Y$  reflect transitions to empty  $e_g$  levels.

In the final state of the Ti 2p x-ray absorption process, the significant overlap of core and valence wave functions is expressed as multiplet effects, which remain largely unscreened in the solid state. These describe primarily atomic effects associated with electronic transitions (intra-ionic transitions) of the general form  $2p^6 d^n \rightarrow 2p^5 d^{n+1}$ . For this reason, they

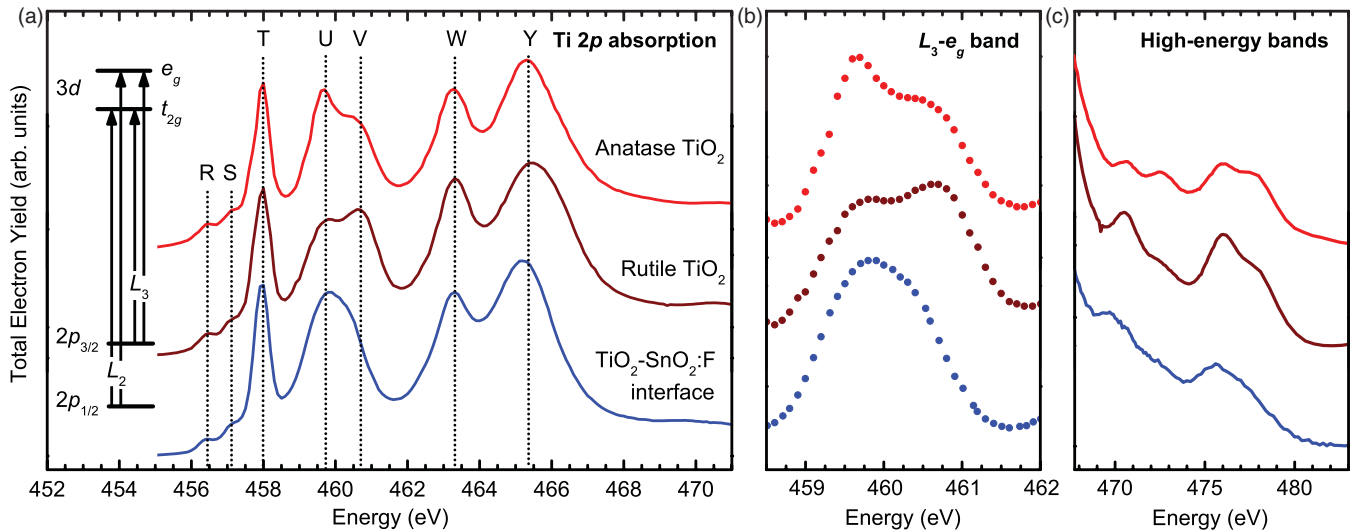


FIG. 4. (Color online) Ti  $L_{2,3}$ -edge x-ray absorption spectra for (top to bottom) anatase TiO<sub>2</sub> (red), rutile TiO<sub>2</sub> (dark red), and TiO<sub>2</sub>-SnO<sub>2</sub>:F (blue). (a) Complete spectra; (b)  $L_3$ - $e_g$  band; (c) high-energy bands, normalized to peak Y. (b) and (c) follow the same order and color convention as in (a).

can be simulated by calculations in the context of atomic multiplet theory with modifications to account for the crystal field and charge transfer effects<sup>48</sup> or through multichannel multiple-scattering calculations.<sup>49</sup> The leading-edge multiplet structure of TiO<sub>2</sub> (peaks R and S), have been assigned in analyses to  $2p^6d^0 \rightarrow 2p^5d^1$  for Ti<sup>4+</sup> in  $O_h$  symmetry.<sup>50</sup> The Ti  $2p$  absorption spectra in Fig. 4(a) indicate the Ti oxidation state in interfacial TiO<sub>2</sub> is primarily 4+.

We now consider the  $L_3$ - $e_g$  band [peaks U and V, Fig. 4(b)], which shows the greatest variation in intensity among the various titanium oxides examined. The  $e_g$  orbitals point directly to the ligands, and as a result the projection of their energy levels in x-ray absorption spectra provides a signature of the cation site environment. It is evident from the comparison of  $L$ -edge spectra provided in Fig. 4(b) that the line shape of the  $L_3$ - $e_g$  band is sensitive to the symmetry of the cation. For all samples the  $e_g$  band is split into an asymmetric doublet, the origins of which have been explained through a number of interpretations. Kucheyev *et al.*<sup>51</sup> discussed these recently in their study of titanium oxide aerogels and through comparisons with amorphous titanium oxide suggested long-range order effects contribute to the line shapes. Based on a negligible change in peak positions with reduction in sample temperature, they also suggested that the dynamic Jahn-Teller effect is not a major contributor to the  $e_g$  band splitting. Calculations of the expected Ti  $L_{2,3}$  absorption-edge shapes performed by Crocombette *et al.*<sup>52</sup> determined that the influence of first-neighbor interactions cannot account for the large  $e_g$  splitting observed in these spectra. This was recently explicitly confirmed in a study by Krüger,<sup>49</sup> which reported Ti  $L_{2,3}$ -edge absorption spectra as simulated by the first-principles multichannel multiple-scattering method, with large numbers of TiO<sub>6</sub> clusters. The splitting of the  $L_3$ - $e_g$  band could only be reproduced after consideration of a cluster size of about 60 atoms, which corresponds to a length scale of  $\sim 1$  nm. This analysis of the  $L_3$ - $e_g$  band suggests that TiO<sub>2</sub>-SnO<sub>2</sub>:F differs in its long-range order from the titanium oxide

reference crystals. The physical correlate to this electronic structure observation could be the structural discontinuity that occurs at the substrate-film interface. Disorder on this length scale could reflect a strain gradient and/or relaxation in the interfacial TiO<sub>2</sub>. The line shape of the  $L_3$ - $e_g$  band appears similar to those found for unrelaxed amorphous TiO<sub>2</sub> prepared by ion bombardment of rutile TiO<sub>2</sub>.<sup>51</sup> These disorder-induced modifications to the interfacial electronic structure are expected to exist within larger crystals deposited onto SnO<sub>2</sub>:F, which would be strained near the interface and relaxed toward bulk properties farther from the interface.

The high-energy region of the Ti  $2p$  absorption spectra, located between 468 and 480 eV [Fig. 4(c)], shows variation among anatase, rutile, and the interfacial TiO<sub>2</sub>. This energy range contains two bands separated by 5–6 eV, which have been suggested to originate from  $2p_{3/2}$  and  $2p_{1/2}$  transitions,<sup>51</sup> as discussed above. The line shapes of these features have been attributed to polaronic transitions,<sup>53</sup> the partial Ti  $3d$  and Ti  $4s$  density of states,<sup>50</sup> and in the molecular orbital description to transitions from Ti  $2p$  core levels to  $t_{1u}$ -type orbitals.<sup>51,54</sup> The peaks' doublet structure, most evident in the spectrum for anatase TiO<sub>2</sub>, is not resolved in the spectrum for TiO<sub>2</sub>-SnO<sub>2</sub>:F. Generally, we observe broadening of the peaks, which is consistent with the disruption of long-range order discussed above with respect to the  $L_3$ - $e_g$  band.

Observation of unique ordering on a length scale of 1 nm in interfacial TiO<sub>2</sub> has a number of implications for carrier transport through the TiO<sub>2</sub>-SnO<sub>2</sub>:F interface during device operation. For example, the corundum crystal structure and associated distorted octahedral symmetry of Ti<sub>2</sub>O<sub>3</sub> causes splitting of conduction band  $t_{2g}$  states into sub-bands in this material.<sup>55</sup> Specifically, in Ti<sub>2</sub>O<sub>3</sub>  $t_{2g}$  states are split into bonding and antibonding  $a_{1g}$  sub-bands, which surround a  $e_g^\pi$  sub-band. This creates a band gap and results in semiconducting behavior. Although these features of the TiO<sub>2</sub>-SnO<sub>2</sub>:F interface cannot be determined from data presented in this paper, it is interesting to consider the interfacial bonding environment

is associated with a number of possible conduction band structures. The unique dispersion of the interfacial Ti  $3d$  band, projected onto O  $p$  orbitals in the O  $1s$  absorption spectrum in Fig. 3, provides additional evidence of the type of long-range order to which these data refer.

#### E. TiO<sub>2</sub>-SnO<sub>2</sub>:F interfaces in solar cells

The data presented in this paper suggest the electronic structure of the TiO<sub>2</sub>-SnO<sub>2</sub>:F interface contrasts with that of its constituent reference crystals through distinct alterations of the crystal field and long-range order of the cation site environment. These observations provide evidence toward understanding the operation of optoelectronic devices utilizing this interface, which often possess feature dimensionality on the length scale over which the interface was probed in this study. For example, dye-sensitized solar cells commonly utilize as electron transport phases colloidal films of TiO<sub>2</sub> nanoparticles whose diameter is on the order of 10 nm.<sup>12</sup> The nature of the TiO<sub>2</sub>-SnO<sub>2</sub>:F interface may play a critical role in determining the performance of these devices. It is generally interpreted that the open-circuit potential of dye-sensitized solar cells is limited by the energy difference between the TiO<sub>2</sub> conduction band and the redox potential of the electrolyte.<sup>56</sup> However, the TiO<sub>2</sub>-SnO<sub>2</sub>:F interface can significantly influence operating parameters such as the fill factor.<sup>57</sup> Rühle and Cahen<sup>57</sup> analyzed the electrostatic potential distribution at the TiO<sub>2</sub>-SnO<sub>2</sub>:F interface and simulated cell performance with an analytical expression for electron tunneling through an electrostatic barrier. The potential distribution from this analysis suggests the existence of a TiO<sub>2</sub>-SnO<sub>2</sub>:F interfacial potential barrier width of approximately 1 nm. This is the same length scale over which we observe distinct dissimilarities between the electronic structure of the interface and those of reference titania crystals. Inorganic solid-state solar cells with similar anode architectures, such as extremely thin absorber cells,<sup>20</sup> require compact TiO<sub>2</sub> thin films to prevent recombination current during operation. In such cells the potential distribution in this layer should be engineered to promote the efficient injection of electrons from TiO<sub>2</sub> into SnO<sub>2</sub>:F. For example, photocurrent transient measurements performed by Rühle and Dittrich<sup>58</sup> suggest increased narrowness of the electrostatic potential drop at the TiO<sub>2</sub>-SnO<sub>2</sub>:F interface may be required to increase the performance of such cells. In most applications, the translation of electrochemical potential of electrons in TiO<sub>2</sub> to an electrostatic potential at the TiO<sub>2</sub>-SnO<sub>2</sub>:F interface<sup>56</sup> is expected to be influenced by the unoccupied density of states studied experimentally in this paper. The description of the electronic structure provided by these measurements suggests, for example, that in nonequilibrium conditions (i.e., solar cell operating conditions), the quasi-Fermi level of electrons in the interface will differ from what is expected by consideration of the respective bulk semiconductor properties of the constituent phases. These observations can also relate to the creation of favorable gradi-

ents of electrical or chemical potential, which could contribute to the observed high efficiency of dye-sensitized solar cells.

#### IV. CONCLUSION

The electronic structure of the TiO<sub>2</sub>-SnO<sub>2</sub>:F interface, an important structure for a number of (opto)electronic devices, has been investigated by soft XAS. The distinct interfacial electronic structure of TiO<sub>2</sub>-SnO<sub>2</sub>:F has been established by contrasting spectra with those for anatase and rutile TiO<sub>2</sub>, SnO<sub>2</sub>:F, and the ZnO-SnO<sub>2</sub>:F and CdO-SnO<sub>2</sub>:F interfaces. The Ti  $3d$  band of the interfacial oxygen  $1s$  absorption spectrum indicates a reduction in the degree of  $p$ - $d$  hybridization and an alteration of the TiO<sub>2</sub> crystal field. Titanium  $2p$  absorption spectra provide evidence for distortion of long-range order around Ti ions in the interfacial TiO<sub>2</sub>.

These observations can inform methodology to address operational deficiencies associated with the TiO<sub>2</sub>-SnO<sub>2</sub>:F interface in optoelectronic devices. For example, a comprehensive characterization of the chemically resolved interfacial electronic structure provides information that facilitates the elimination of unfavorable processing conditions, including high temperatures, which are associated with additional costs and diffusion effects between phases, and which preclude the use of inexpensive temperature-sensitive substrates. The results indicate that in solar cell operating conditions, the quasi-Fermi level of electrons in the interface will differ from predictions based on bulk oxide material properties. The interfacial electronic structure in addition influences the electrostatic potential distribution at the oxide-TCO interface, which is often a critical operational aspect of working optoelectronic devices. The description of the unoccupied electronic states at the TiO<sub>2</sub>-SnO<sub>2</sub>:F interface presented in this report provides additional information toward explaining deviations in solar cell performance metrics from those expected by bulk material properties and the various predictive models.

#### ACKNOWLEDGMENTS

This research has been supported by the US Department of Energy, Office of Energy Efficiency and Renewable Energy and Office of Basic Science under Contract No. DE-AC02-05CH11231. M.K. acknowledges support from both the Swedish Research Council (VR) and Axel Hultgren's memorial fund. The ALD was carried out within the Center on Nanostructuring for Efficient Energy Conversion at Stanford University, an Energy Frontier Research Center funded by the US Department of Energy, Office of Science, Office of Basic Energy Sciences under Grant No. DE-SC0001060. J.R.B. acknowledges funding from the Department of Defense (DoD) through the National Defense Science and Engineering Graduate (NDSEG) Fellowship and from the National Science Foundation (NSF) Graduate Fellowship under Grant No. DGE-0645962.

\*lionelv@xjtu.edu.cn

†ssmao@lbl.gov

<sup>1</sup>P. Zubko, S. Gariglio, M. Gabay, P. Ghosez, and J.-M. Triscone, *Annu. Rev. Condens. Matter Phys.* **2**, 141 (2011).

<sup>2</sup>B. A. Gregg, *J. Phys. Chem. B* **107**, 4688 (2003).

<sup>3</sup>A. J. Nozik, *Nano Lett.* **10**, 2735 (2010).

<sup>4</sup>J. Chakhalian, J. W. Freeland, H.-U. Haberman, G. Cristiani, G. Khaliullin, M. van Veenendaal, and B. Keimer, *Science* **318**, 1114 (2007).

<sup>5</sup>A. Ohtomo and H. Y. Hwang, *Nature* **427**, 423 (2004).

- <sup>6</sup>A. Brinkman, M. Huijben, M. van Zalk, J. Huijben, U. Zeitler, J. C. Maan, W. G. van der Wiel, G. Rijnders, D. H. A. Blank, and H. Hilgenkamp, *Nat. Mater.* **6**, 493 (2007).
- <sup>7</sup>C. X. Kronawitter, J. R. Bakke, D. A. Wheeler, W.-C. Wang, C. Chang, B. R. Antoun, J. Z. Zhang, J.-H. Guo, S. F. Bent, S. S. Mao, and L. Vayssieres, *Nano Lett.* **11**, 3855 (2011).
- <sup>8</sup>L. Vayssieres, *J. Phys. Chem. C* **113**, 4733 (2009).
- <sup>9</sup>L. Vayssieres, C. Persson, and J.-H. Guo, *Appl. Phys. Lett.* **99**, 183101 (2011).
- <sup>10</sup>L. Vayssieres, C. Sathe, S. M. Butorin, D. K. Shuh, J. Nordgren, and J.-H. Guo, *Adv. Mater.* **17**, 2320 (2005).
- <sup>11</sup>P. Ardalan, T. B. Brennan, H. B. R. Lee, J. R. Bakke, I. K. Ding, M. D. McGehee, and S. F. Bent, *ACS Nano* **5**, 1495 (2011).
- <sup>12</sup>M. Grätzel, *Inorg. Chem.* **44**, 6841 (2005).
- <sup>13</sup>N. Tétreault, É. Arsenaault, L.-P. Heiniger, N. Soheilnia, J. Brillet, T. Moehl, S. Zakeeruddin, G. A. Ozin, and M. Grätzel, *Nano Lett.* **11**, 4579 (2011).
- <sup>14</sup>M.-H. Kim and Y.-U. Kwon, *J. Phys. Chem. C* **113**, 17176 (2009).
- <sup>15</sup>K. S. Leschkies, R. Divakar, J. Basu, E. Enache-Pommer, J. E. Boercker, C. B. Carter, U. R. Kortshagen, D. J. Norris, and E. S. Aydil, *Nano Lett.* **7**, 1793 (2007).
- <sup>16</sup>A. K. K. Kyaw, X. W. Sun, C. Y. Jiang, G. Q. Lo, D. W. Zhao, and D. L. Kwong, *Appl. Phys. Lett.* **93**, 221107 (2008).
- <sup>17</sup>K. Ernst, A. Belaidi, and R. Könenkamp, *Semicond. Sci. Technol.* **18**, 475 (2003).
- <sup>18</sup>C. Lévy-Clément, R. Tena-Zaera, M. A. Ryan, A. Katty, and G. Hodes, *Adv. Mater.* **17**, 1512 (2005).
- <sup>19</sup>T. Jiang, T. Xie, Y. Zhang, L. Chen, L. Peng, H. Li, and D. Wang, *PhysChemChemPhys.* **12**, 15476 (2010).
- <sup>20</sup>R. Könenkamp, R. C. Word, and C. Schlegel, *Appl. Phys. Lett.* **85**, 6004 (2004).
- <sup>21</sup>*On Solar Hydrogen & Nanotechnology*, edited by L. Vayssieres (Wiley, Singapore, 2009), pp. 1–680.
- <sup>22</sup>L. Vayssieres, *Adv. Mater.* **15**, 464 (2003).
- <sup>23</sup>T. Ma, M. Guo, M. Zhang, Y. Zhang, and X. Wang, *Nanotechnology* **18**, 035605 (2007).
- <sup>24</sup>K. Zhu, E. A. Schiff, N.-G. Park, J. van de Lagemaat, and A. J. Frank, *Appl. Phys. Lett.* **80**, 685 (2002).
- <sup>25</sup>Y. Ling, G. Wang, D. A. Wheeler, J. Z. Zhang, and Y. Li, *Nano Lett.* **11**, 2119 (2011).
- <sup>26</sup>S. Gutmann, M. A. Wolak, M. Conrad, M. M. Beerbom, and R. Schlaf, *J. Appl. Phys.* **109**, 113719 (2011).
- <sup>27</sup>J. T. Tanskanena, J. R. Bakke, T. A. Pakkanen, and S. F. Bent, *J. Vac. Sci. Technol. A* **29**, 031507 (2011).
- <sup>28</sup>V. E. Henrich, *Rep. Prog. Phys.* **48**, 1481 (1985).
- <sup>29</sup>G. Korotcenkov, *Mater. Sci. Eng. B* **139**, 1 (2007).
- <sup>30</sup>J.-H. Guo, L. Vayssieres, C. Persson, R. Ahuja, B. Johansson, and J. Nordgren, *J. Phys. Condens. Matter* **14**, 6969 (2002).
- <sup>31</sup>J. Lahiri, S. Senanayake, and M. Batzill, *Phys. Rev. B* **78**, 155414 (2008).
- <sup>32</sup>L. F. J. Piper, L. Colakerol, P. D. C. King, A. Schleife, J. Zúñiga-Pérez, P.-A. Glans, T. Learmonth, A. Federov, T. D. Veal, F. Fuchs, V. Muñoz-Sanjosé, F. Bechstedt, C. F. McConville, and K. E. Smith, *Phys. Rev. B* **78**, 165127 (2008).
- <sup>33</sup>F. M. F. de Groot, M. Grioni, J. C. Fuggle, J. Ghijsen, G. A. Sawatzky, and H. Petersen, *Phys. Rev. B* **40**, 5715 (1989).
- <sup>34</sup>M. Abbate, F. M. F. de Groot, J. C. Fuggle, A. Fujimori, O. Strebel, F. Lopez, M. Domke, G. Kaindl, G. A. Sawatzky, M. Takano, Y. Takeda, H. Eisaki, and S. Uchida, *Phys. Rev. B* **46**, 4511 (1992).
- <sup>35</sup>C. McGuinness, C. B. Stagarescu, P. J. Ryan, J. E. Downes, D. Fu, K. E. Smith, and R. G. Egdell, *Phys. Rev. B* **68**, 165104 (2003).
- <sup>36</sup>J. Chouvin, J. Olivier-Fourcade, J. C. Jumas, B. Simon, Ph. Biensan, F. J. Fernández Madrigal, J. L. Tirado, and C. Pérez Vicente, *J. Electroanal. Chem.* **494**, 136 (2000).
- <sup>37</sup>H. Thakur, R. Kumar, P. Thakur, N. B. Brookes, K. K. Sharma, A. P. Singh, Y. Kumar, S. Gautam, and K. H. Chae, *Chem. Phys. Lett.* **511**, 322 (2011).
- <sup>38</sup>K. C. Mishra, K. H. Johnson, and P. C. Schmidt, *Phys. Rev. B* **51**, 13972 (1995).
- <sup>39</sup>S. O. Kucheyev, T. F. Baumann, P. A. Sterne, Y. M. Wang, T. van Buuren, A. V. Hamza, L. J. Terminello, and T. M. Willey, *Phys. Rev. B* **72**, 035404 (2005).
- <sup>40</sup>H.-J. Ahn, H.-C. Choi, K.-W. Park, S.-B. Kim, and Y.-E. Sung, *J. Phys. Chem. B* **108**, 9815 (2004).
- <sup>41</sup>X. T. Zhou, J. G. Zhou, M. W. Murphy, J. Y. P. Ko, F. Heigl, T. Regier, R. I. R. Blyth, and T. K. Sham, *J. Chem. Phys.* **128**, 144703 (2008).
- <sup>42</sup>X. T. Zhou, F. Heigl, M. W. Murphy, T. K. Sham, T. Regier, I. Coulthard, and R. I. R. Blyth, *Appl. Phys. Lett.* **89**, 213109 (2006).
- <sup>43</sup>L. Soriano, M. Abbate, J. Vogel, J. C. Fuggle, A. Fernández, A. R. González-Elipe, M. Sacchi, and J. M. Sanz, *Surf. Sci.* **290**, 427 (1993).
- <sup>44</sup>D. W. Fischer and W. L. Baun, *J. Appl. Phys.* **39**, 4757 (1968).
- <sup>45</sup>F. M. F. de Groot, M. O. Figueiredo, M. J. Basto, M. Abbate, H. Petersen, and J. C. Fuggle, *Phys. Chem. Miner.* **19**, 140 (1992).
- <sup>46</sup>A. G. Thomas, W. R. Flavell, A. K. Mallick, A. R. Kumarasinghe, D. Tsoutsou, N. Khan, C. Chatwin, S. Rayner, G. C. Smith, R. L. Stockbauer, S. Warren, T. K. Johal, S. Patel, D. Holland, A. Taleb, and F. Wiame, *Phys. Rev. B* **75**, 035105 (2007).
- <sup>47</sup>X. Chen, P.-A. Glans, X. Qiu, S. Dayal, W. D. Jennings, K. E. Smith, C. Burda, and J.-H. Guo, *J. Electron Spectros. Relat. Phenomena* **162**, 67 (2008).
- <sup>48</sup>H. Ikeno, F. M. F. de Groot, E. Stavitski, and I. Tanaka, *J. Phys. Condens. Matter* **21**, 104208 (2009).
- <sup>49</sup>P. Krüger, *Phys. Rev. B* **81**, 125121 (2010).
- <sup>50</sup>L. D. Finkelstein, E. I. Zabolotzky, M. A. Korotin, S. N. Shamin, S. M. Butorin, E. Z. Kurmaev, and J. Nordgren, *X-Ray Spectrom.* **31**, 414 (2002).
- <sup>51</sup>S. O. Kucheyev, T. van Buuren, T. F. Baumann, J. H. Satcher Jr., T. M. Willey, R. W. Meulenberg, T. E. Felter, J. F. Poco, S. A. Gammon, and L. J. Terminello, *Phys. Rev. B* **69**, 245102 (2004).
- <sup>52</sup>J. P. Crocombette and F. Jollet, *J. Phys. Condens. Matter* **6**, 10811 (1994).
- <sup>53</sup>G. van der Laan, *Phys. Rev. B* **41**, 12366 (1990).
- <sup>54</sup>J. A. Tossell, D. J. Vaughan, and K. H. Johnson, *Am. Mineral.* **59**, 319 (1974).
- <sup>55</sup>A. T. Paxton and L. Thiên-Nga, *Phys. Rev. B* **57**, 1579 (1998).
- <sup>56</sup>J. Bisquert, D. Cahen, G. Hodes, S. Rühle, and A. Zaban, *J. Phys. Chem. B* **108**, 8106 (2004).
- <sup>57</sup>S. Rühle and D. Cahen, *J. Phys. Chem. B* **108**, 17946 (2004).
- <sup>58</sup>S. Rühle and T. Dittrich, *J. Phys. Chem. B* **109**, 9522 (2005).